Thermal characterization of a nematic liquid crystal suited for the fabrication of NIR spectrally-tunable vertical cavity surface emitting lasers

ANDREA SIMAZ,[1,2] BENJAMIN BOISNARD,[1] JEAN-BAPTISTE DOUCET,[1] THIERRY CAMPS,[1] BENJAMIN REIG,[1] JULIEN LUMEAU,[4] ◉ THOMAS BEGOU,[4] ALBERTO TIBALDI,[2,3] ◉ PIERLUIGI DEBERNARDI,[3] AND VÉRONIQUE BARDINAL[1,*]

[1]*Univ Toulouse, CNRS, LAAS, 7 Ave Colonel Roche, F-31400 Toulouse, France*
[2]*Department of Electronics and Telecommunications, Politecnico di Torino, 10129 Turin, Italy*
[3]*CNR-IEIIT c/o Politecnico di Torino, 10129 Turin, Italy*
[4]*Aix Marseille Univ, CNRS, Centrale Marseille, Institut Fresnel, Marseille, France*
[*]*bardinal@laas.fr*

Abstract: In this work, the thermo-optical properties of a nematic liquid crystal are determined through reflectance measurements performed on a high finesse tunable filter fabricated using a polymer-based microcell technology. The final aim is to insert such material in the optical cavity of a 850 nm tunable VCSEL device, in which local self-heating due to CW pumping must be taken into account. These localized interferometric experiments are performed in the near-infra-red range and at temperatures up to 115 °C. A thermal model is derived from the acquired data. Finally, we demonstrate that the birefringence of QYPDLC-36 liquid crystal remains higher than 0.18 at 60 °C, feature well suited to real device operation.

1. Introduction

Vertical-cavity surface-emitting lasers (VCSELs) are nowadays key laser sources in the fields of optical communications and sensors. This is due to their numerous advantages such as longitudinal single-mode emission, circular beam shape, low-power consumption and collective fabrication. To further extend their use in new applications such as gas sensing, optical coherence tomography (OCT) imaging or miniaturized spectroscopy, wavelength tunability is required. The classical approach to obtain a spectrally-tunable VCSEL is based on the modification of the physical cavity length using a micro electrical-mechanical system (MEMS) [1]. An alternative method is rather to change the refractive index of the cavity. This approach exploits an intracavity liquid crystal (LC) layer, thus avoiding any moving part in the device. Additionally, in the Near-Infrared range, the liquid crystal absorption coefficient is low [2], essential feature to ensure a low laser threshold gain and limit the thermal effects. A tunable room temperature continuous wave (CW) lasing was recently reported in an optically-pumped 1.55 μm VCSEL integrating a new kind of LC polymer microcell [3] indicating a good photostability of the used LC (standard E7 from Merck). However, the tuning range was limited to 23.5 nm, mainly due to the decrease of the E7 birefringence [4]. In a VCSEL, the local temperature can typically reach 60 °C due to self-heating under CW pumping [5]. In this work, the optical properties of a LC having better thermal properties than E7, QYPDLC-036 [6], similar to BL-036 from Merck, are characterized using an interference measurement method.

2.   Methodology for LC index measurement

2.1.   Existing methods

Many studies have been devoted to liquid crystals optical characterization since the precise knowledge of the anisotropic optical constants is crucial for the design of LC-based electro-optic devices. For the case of a tunable LC-VCSEL, it is mandatory to know these data and their temperature dependence in the NIR range [4]. However, only few data have been published so far. In fact, most of the possible methods are difficult to implement on birefringent materials and with a temperature variation.

A first measurement technique exploits an Abbe refractometer, which is a very accurate equipment to measure the refractive index. Li et al. [7] first exploited this method coupled to a Peltier stage to measure the refractive index of E7 at temperatures from 15 to 50 °C and at discrete wavelengths ranging from 450 nm to 656 nm with a precision of 0.7%. However, this kind of measurement is limited to the visible spectrum. Another method would be the usage of a Talbot-Rayleigh refractometer which extends the previous range to 820 nm [8] and it was used to study the refractive indices of 5CB LC. To further extend towards longer wavelengths it is also possible to exploit a wedged LC cell using a refractometric wedge method (RWM) [7,9]. This more complex configuration was used by Li et al. to obtain the thermal dependence of E7 refractive indices at 1.55 μm and 10.6 μm. However, the precision was lower because the measurement is very sensitive to the accuracy of the geometric alignment and the control of the wedge angle.

Another approach consists in using a spectroscopic ellipsometry set-up (SE) with extended operation range in the NIR. This instrument measures the change in the polarization state of a beam of light upon reflection from the sample of interest. This variation in the polarization state is a function of the thickness and the refractive index of the material under investigation. A beam of linearly polarized light incident on the sample's surface creates a reflection. This reflection is composed by a perpendicular component (E_s), and a parallel one (E_p) and both the phase and the amplitude of the reflected wave depend on the optical properties of the sample. The ratio between the amplitude and phase (Ψ and Δ) serves as input data to extract the refractive index of the material by using a data inversion procedure based on the multilayer Fresnel theory [10]. Nevertheless, the physical model should be well defined; otherwise, the measurement are invalid. For this kind of reason, simple measurement with solid samples becomes very complicated using LC. Moreover this method is very sensitive to surface roughness and alignment uncertainties. A solution to improve the precision is to couple SE to a half-leaky guided mode technique (HLGM) using a specific waveguide and a prism, as done by V. Tkachenko et al. [11]. With these combined techniques, the refractive index of 5CB LC and its thermal variation could be measured from 200 nm to 1700 nm with a precision of 10^{-4}. The pretilt angle and the anchoring strength could be also determined using additional procedures. However, this complex method requires the fabrication of specific waveguiding cells and dedicated holders.

Finally, an alternative method based on a microfiber-assisted Mach-Zehnder interferometer (MAMZI) was reported by Xie et al [12] for the characterization of E7 LC enclosed in a capillary tube in a wavelength range between 1250 and 1700 nm and up to 100 °C. However, with this method, it is not possible to measure the value of the LC extraordinary index for the alignment configuration corresponding to a real device, i.e. with the same pre-tilt angle.

Optical interference methods appear easier to implement than the above-mentioned techniques as they can be directly applied to tunable optical LC-filters that better reflect a real device configuration. Kawaida et al. first measured the optical indices of a ferroelectric SmC* phase LC and corresponding thermal variation by analyzing the Fabry-Perot fringes observed in the transmission spectra of a FPI filter (Fabry-Perot Interferometer). To this aim, these authors used a LC-cell having two semi-transparent aluminum inner coatings to improve the signal contrast

[13]. More recently, Ozaki *et al.* implemented the same method using an optical microscope connected to two different spectrometers and replacing aluminium by a less absorbing metal, silver [14]. The refractive index of 5CB could be this way extracted in a spectral range from 400 nm to 1273 nm. However, the use of thin metallic layers in the LC-cell makes the signal fitting difficult, as it is strongly dependent on the absorption of these layers. Moreover, the use of two rubbed layers for LC alignment can also alter the precision of the measurement as homogeneity and LC director axis are not very well controlled.

Here, we applied a similar technique but used a high-finesse FPI composed of two dielectric distributed mirrors (DBRs) having the advantages of being lossless and highly reflective over a spectral band wide enough to allow the observation of at least four interference peaks. This was done at room temperature by E. Miszczyk et al. on standard macrocells [15]. Here, the used LC-filters include for the first time microcells and a single LC alignment layer made of a nano-structured grating fabricated with a nanoimprinting technique [16]. The wafer-scale homogeneity of this nanograting is very high as the maximal variation of the depth and the width of the grating lines, along which the LC molecules are oriented is lower than 2 nm over a distance of 4 inches. Additionally, the homogeneity of our LC cell height is better than 3% over the sample which is not achievable in a conventional macrocell assembled with glue and no complex positioning procedure is thus necessary for guaranteeing the measurement repeatability. Another key advantage of our approach is to use a FTIR spectrometer (Fourier Transform Infra-Red) rather than a conventional spectrometer. This set-up offers a much higher spectral resolution (better than 0.2 nm) and it can cover a wider spectral range (500 nm–20 μm). This set-up is equipped with a microscope stage allowing the acquisition of localized reflectance spectra at a quasi-normal incidence angle (5∘) using a small numerical aperture objective and with a high spatial resolution (better than 400 μm^2). It is also fully compatible with the use of a thin Peltier stage, making thermal measurements easy.

Finally, it is also worth noting that the FPI filters measured here include the same LC-microcells that will be integrated in our tunable LC-VCSELs. Therefore, it will be possible to directly exploit the extracted optical data for further optimizing the opto-thermal design of these devices.

Using this new characterization method, the optical properties of two LCs, QYPDLC-07 and QYPDLC-036 [6], which are similar to Merck E7 and Merck BL-036 respectively, are measured for the first time around a wavelength of interest for active photonic LC-devices (850 nm) and at temperatures varying from 25 °C to 115 °C. A preliminary study was led by the authors on a 1.55 μm filter with mirrors having a moderate reflectivity level to evaluate the feasibility of the measurement [17]. Here we demonstrate the efficiency of the method for index determination thanks to the fabrication and the use of 850 nm high finesse LC filters.

2.2. Localized reflectance measurements on a high finesse tunable filter

In this work, high finesse 850 nm tunable optical micro-filters were first fabricated and filled with QY-PDLC-007 or QY-PDLC-036. The choice of these LCs was driven by their high birefringence but also their sufficiently low viscosity to make fabrication feasible. Their thermo-optical behavior was then studied through localized reflectance measurements at different temperatures. A cross section of a typical filter is shown in Fig. 1(a). The device is composed of two identical dielectric distributed Bragg reflectors deposited on two ITO/fused silica substrates (Table 1). The 850 nm DBRs are deposited using plasma assisted reactive magnetron sputtering (Bühler HELIOS) and made of 7.5x(Nb_2O_5/SiO_2) pairs with a reflectivity higher than 99.75% [18]. An antireflection coating is deposited on the back side of each mirror sample. A LC alignment grating is first imprinted in a SU-8 thin layer (900 nm) on the surface of one of the mirrors. The polymer walls of the LC cell are defined in a thick Perminex photoresist layer deposited on the surface of the second mirror and patterned by standard UV photolithography. The two parts are then sealed together using a thermal printing set-up and exploiting the self-sealing properties of this resist.

The LC thickness is fixed by the height of the polymer wall. A top view of the 9 fabricated LC microcells is shown in Fig. 1(b). More details on fabrication can be found elsewhere [3,16].
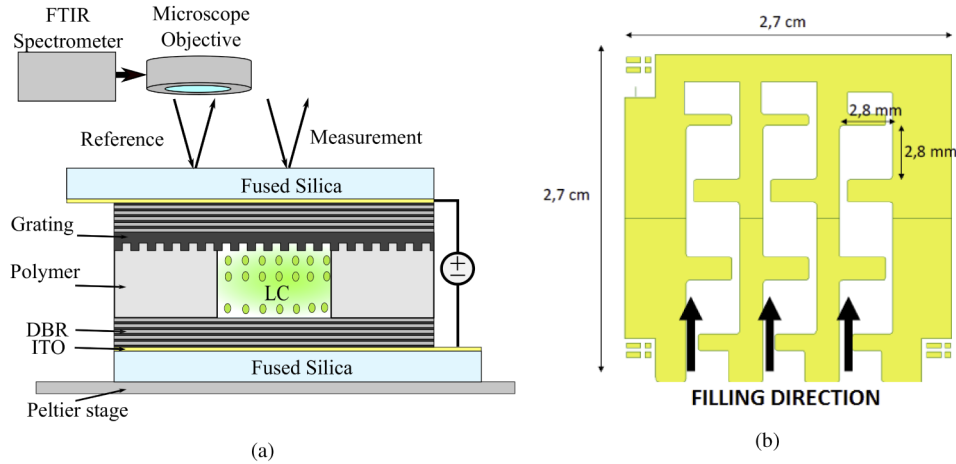

Fig. 1. (a) Cross-section of the fabricated tunable filter including a nanoimprinted grating for LC alignment and schematic of the used experimental set-up. After thermal calibration on an empty cell, the thermo-optical measurements are made on a filled microcell. (b) top view of the LC microcells design.

Table 1. 1D cross-section of the analyzed structure.

Building Block	Material	n(850 nm)	L [nm]
Antireflection coating	Nb$_2$O$_5$/SiO$_2$	2.281/1.471	28/186
Substrate	Fused silica [22]	1.45	1×10^6
LC electrode	ITO	1.717-i0.015	139
7.5 pairs Top DBR	Nb$_2$O$_5$[23]/SiO$_2$[24]	2.281/1.471	92.1/142.8
Grating section	SU-8 2000 [20]	1.56	900
LC reservoir	Perminex2000 [21]	1.58	2700
7.5 pairs Top DBR	Nb$_2$O$_5$/SiO$_2$	2.281/1.471	92.1/142.8
LC electrode	ITO	1.717-i0.015	139
Substrate	Fused silica	1.45	1×10^6
Antireflection coating	Nb$_2$O$_5$/SiO$_2$	2.281/1.471	28/186

The FTIR set-up used in this study is a VERTEX 70 (Bruker Optics) equipped with a Quartz beamsplitter coupled with a Si-diode photodetector (SiD 510) for the Near Infrared Range (NIR) measurement between 600 nm and 1100 nm. We used a low numerical aperture (x4) to perform these measurements. In order to heat the device under test and precisely know the applied temperature, a Linkam heat controller (TMS 94) connected with a temperature-controlled stage (LTS 350) was used.

The principle of the measurement is the following: a first localized reflectance spectrum is acquired on the wall of a cell, as a reference. We have checked before our experiments that the thermal change of the peaks of an empty cell is similar to the one measured on the polymer wall located close to it. The Perminex refractive index thermal change was therefore neglected compared to the change of the physical thickness due to Perminex thermal dilatation and to the thermal variation in the DBRs. As seen on the example measured at room temperature for a 850

nm filter in Fig. 2(a), 5 successive sharp resonances can be clearly observed in the stop band, with a Free Spectral Range (FSR) of 47 nm for the modes closest to 850 nm, in good agreement with modelling. A second measurement is then made at the center of the LC-microcell. As expected, due to the LC anisotropy, the resonance modes of each order are split in two, corresponding to ordinary and extraordinary polarizations (Fig. 2(a)). The discrimination between these modes can be done by simply inserting a polarizer on the optical path.
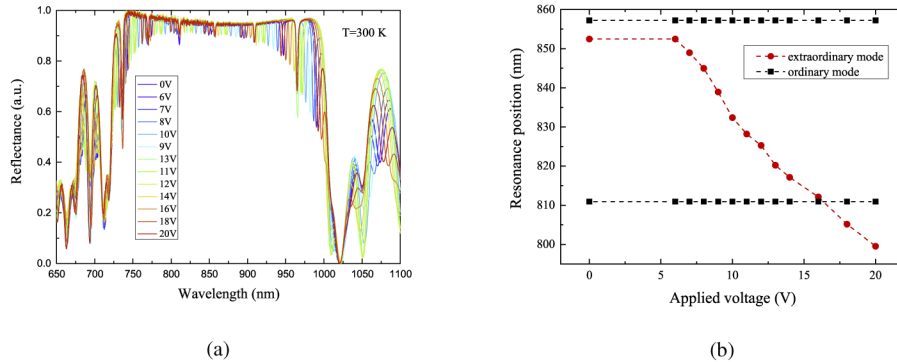

Fig. 2. (a) Localized reflectance spectra of the LC cell measured at room temperature as a function of the applied voltage. (b) Tuning curve measured for the extraordinary mode positioned closest to the central wavelength (850 nm/LC : QYPDLC-036).

The electro-optical behavior of the filter was checked at room temperature by applying a voltage between the ITO electrodes. As expected, the spectral position of the extraordinary modes are blue-shifted above the Fréedericksz transition, corresponding to a voltage threshold of ~ 6 V (Fig. 2(b)) whereas the ordinary modes position remains constant. For the extraordinary mode closest to 850 nm, a continuous tuning range (TR) of 52 nm can be observed for 20 V applied with no mode hopping.

3.   Thermal measurements

In the following, the applied voltage is now kept at 0 V and the temperature is varied to mimic a self-heating in the device. To this aim, the filter is placed on a slim Peltier holder inside the microscope stage of a FTIR spectrometer. In this way, localized reflectance spectra can be precisely measured on the cell, from room temperature to 115 °C in uniform steps of 5.00±0.01) °C and a non-uniform step close to the clearing temperature.

3.1.   Thermal variation of peaks resonances of the reference

As above mentioned, a reference measurement is made on the wall of the microcell for each temperature to take into account the thermal expansion of the polymer layers present in the multilayer stack, namely the 2.7 μm-thick polymer wall of the LC microcell, and to a much smaller extent, the 900 nm-thick SU-8 layer used for the LC alignment grating fabrication (Fig. 1(a)). This way, the thermal effects occurring in the whole multilayer stack can be differentiated from those taking place only in the LC layer. As seen in Fig. 3(a), a temperature increase of 90 °C leads to a spectral red-shift of 16 nm. A calibration law for the thermal expansion of the cell height can be extracted from these results (Fig. 3(b)).

3.2.   Thermal variation of peaks resonances of the LC cell

Once the reference measurements are done, the filter resonance positions are acquired in the cell as a function of the temperature. The results are plotted for both ordinary (o) and extraordinary
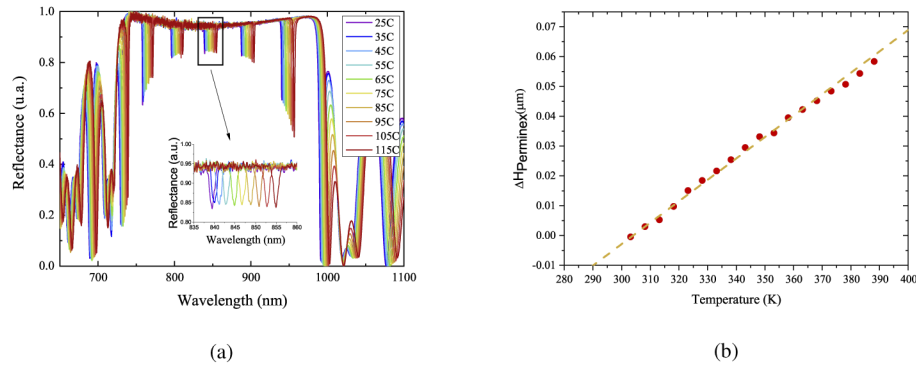
(a)

(b)

Fig. 3. (a) Reflectance spectra of the reference as a function of the temperature displayed with 10 $^\circ$C step for sake of clarity. (b) Thermal calibration law extracted from the reference measurements ($\Delta H_{Perminex}(T) = \frac{\Delta\lambda(T)}{\lambda_0} * H_{Perminex}$ where is found to be $\Delta H_{Perminex}(T) = 7.18 * 1e^{-4}T - 0.21828$).

(e) polarizations in Fig. 4(b). The uncertainty is calculated through propagation error theory and is mainly given by the wavelength resolution of the FTIR spectrometer and the temperature resolution of the Peltier stage. The total relative error is found to be 0.25% and it is shown on the figure through the error-bar along the y axis (Fig. 4(b)).
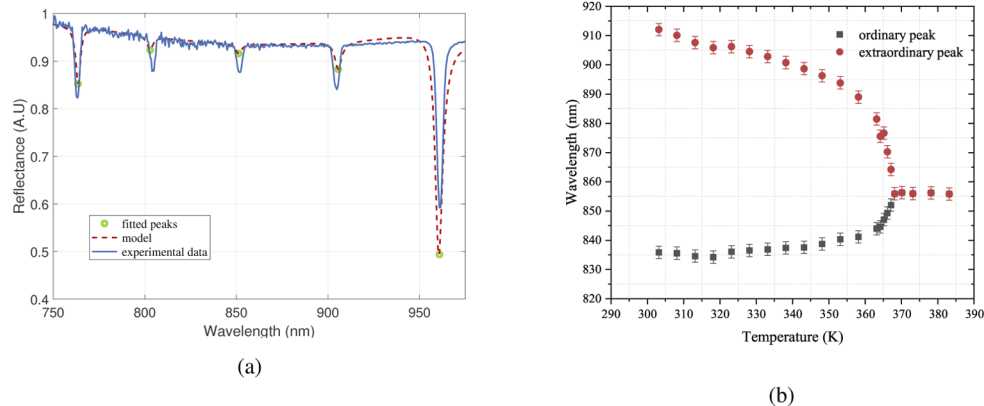

(a)

(b)

Fig. 4. (a) Measured (blue) and calculated from fitting (red) reflectance spectra (b) Spectral positions of the ordinary and extraordinary modes close to 850 nm extracted from the measurements (QYPDLC-036).

4.   Modelling and refractive index model extraction

4.1.   Device modelling

The device has been modelled using a transfer matrix method (TMM) coupled with an RCWA code for the grating analysis [19]. The material dispersion has been taken into account in the analysis and the material parameters were taken from [20–24] and from ellipsometry measurements. The code has been implemented in MATLAB [25]. The main purpose of this code is to convert the wavelength dependence of the spectra of the liquid crystal to the refractive index dependence of the same. To this aim, the modeled reflectance curve and the experimental data are compared (see Fig. 4(a)). First of all, the grating effect on the LC polarization has been analyzed. Simulations

showed that the grating does not affect the reflectivity of the filter. Hence, to speed up the modeling, the grating has been suppressed. The fitting of the reflectance spectra consists of two steps; in the first step, the unknown value of the Perminex and SU-8 heigths is determined by exploiting a global optimizer algorithm that minimizes the error function on the empty cell. In that way, the unknown LC refractive index values are replaced by the known Perminex refractive index value. In the second step, once the precise values of the Perminex wall's height and the SU8 thickness are known, the code is run for each polarization to determine the independent values of n_e and n_o. In fact, at normal incidence, the two extraordinary and ordinary peaks are independent. The model fitting reproduces very well the reflectance spectra for each considered temperature and the χ^2 values are found to be lower than 5% [26].

4.2. Derived refractive indices

The corresponding values of refractive index for both extraordinary and ordinary polarizations n_e and n_o can be extracted from the above-described fitting. The evolution of the approximated average index value $n \simeq (2n_o + n_e)/3$ can be also calculated from these data. It identifies a sort of equivalent refractive index as if the material was isotropic. As seen in Fig. 5(a), the extraordinary index and the average index values decrease with the temperature, whereas the ordinary one remains almost constant below 350 K ($\simeq 75$ °C). As expected, the birefringence Δn = $n_e - n_o$ dramatically falls when the temperature is close to the clearing temperature Tc which is found to be equal to 95 °C (Fig. 5(b)). This has to be compared to the maximal temperature of only 58.5 °C we measured on another filter filled with QYPDLC-07, a LC very similar to E7. Moreover, the birefringence of QYPDLC-036 remains significant at 60 °C ($\Delta n = 0.1861$). This demonstrates that it can be exploited for the design of a widely-tunable LC-VCSEL device submitted to high density optical or electrical injection.
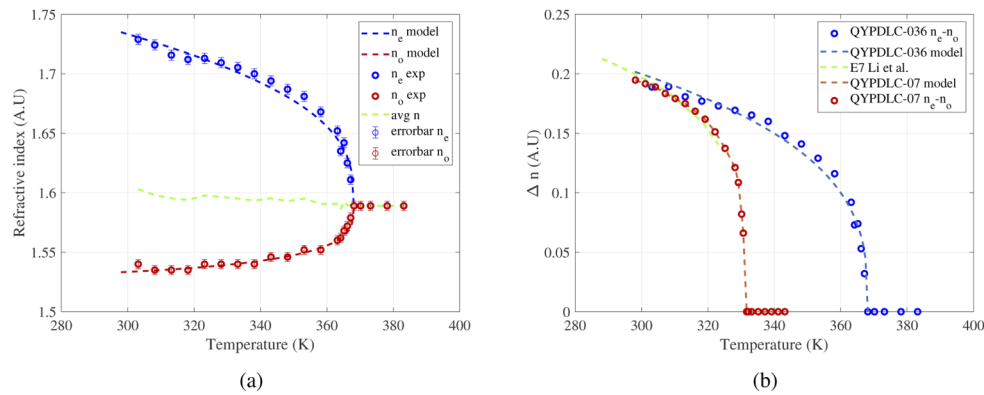

Fig. 5. (a) Refractive indices (squares: measured/ dotted line: model/blue: extraordinary/ red: ordinary/ green: average) as a function of the temperature (QYPDLC-036) (b) birefringence comparison between QYPDLC-036 (blue circles: measured/ blue dotted line: model), QYPDLC-07 (red circles: measured/ blue dotted line: model) [17] and Merck E7 birefringence (extracted from the literature/ green dotted line) [7].

4.3. Thermal model extracted from the data

To derive a precise model for both extraordinary and ordinary indices, the thermal variation below Tc is described using the following four-parameter model [7]:

$$n_e(T) = A - BT + 2/3(\Delta n)_0 \left(1 - \frac{T}{T_C}\right)^{\beta} \tag{1}$$

$$n_o(T) = A - BT - 1/3(\Delta n)_0 \left(1 - \frac{T}{T_C}\right)^\beta \tag{2}$$

where $(\Delta n)_0$ is the LC birefringence at T=0 K and β a material constant. $(\Delta n)_0$ and β can be extracted by fitting the difference between the $n_e(T)$ and n_o (T) curves:

$$(1) - (2) \quad (\Delta n)_T = n_e(T) - n_o(T) = (\Delta n)_0 \left(1 - \frac{T}{T_C}\right)^\beta \tag{3}$$

A and B parameters can be derived from the fitting of the average value of the refractive index $\langle n \rangle$:

$$A(T) + B(T)T = \langle n \rangle = (n_e + 2n_o)/3 \tag{4}$$

The corresponding fitting results are reported in Table 2.

Table 2. Thermal parameters extracted from the fitting of experimental data.

	λ (μm)	$T_c(K)$	**A**	**B**(K^{-1})	$(\Delta n)_0$	β
QYPDLC-07	0.850	331.65	1.76506	6.52*1e-4	0.36046	0.25534
QYPDLC-36	0.850	367.15	1.65575	1.85*1e-4	0.34636	0.32608

In Fig. 5(a), the fitted thermal curve is shown with the experimental points for n_e, n_o and n average, while in Fig. 5(b) the birefringence of E7 LC at 850 nm measured by Li et al. is compared to QYPDLC-036 measured with our method. It can be clearly seen a high value of birefringence is obtained for a much higher temperature if QYPDLC-036 is adopted. Finally, these index models can be used to reproduce the real operation of 850 nm LC tunable active photonic devices.

5. Conclusions

A simple method for determining the refractive indices of a liquid crystal as a function of the temperature is developed. It is based on localized reflectance measurements performed by FTIR microscopy from 20 °C to 110 °C on a tunable high finesse filter including a polymer-based LC microcell. It gives access to reliable LC indices values at the filter resonance wavelength (850 nm in this work). A birefringence higher than 0.18 at 60 °C is measured for QYPDLC-036, for the first time in this spectral range, proving this LC is a good candidate for an insertion in a LC tunable VCSEL. Future work will concern the extension of the measurement to shorter and longer wavelengths to derive a dispersion law for all the considered temperatures, the design of a 850 nm widely-tunable LC-VCSEL using this material and corresponding models, as well as its fabrication with the polymer microcell technology.

Disclosures. The authors declare no conflicts of interest.

Data availability. Data on the codes underlying the results presented in this paper are available in Ref. [19–25].

References

1. P. Qiao, K. Cook, K. Li, and C. Chang-Hasnain, "Wavelength-swept VCSELs," IEEE J. Sel. Top. Quantum Electron. **23**(6), 1–16 (2017).
2. S.-T. Wu, "Absorption measurements of liquid crystals in the ultraviolet, visible, and infrared," J. Appl. Phys. **84**(8), 4462–4465 (1998).
3. B. Boisnard, M. Alouini, P. Debernardi, V. Bardinal, C. Levallois, C. Paranthoen, S. Pes, T. Camps, B. Sadani, K. Tavernier, S. Bouchoule, and L. Dupont, "Cw operation of a tunable 1550 nm VCSEL integrating liquid-crystal microcells," IEEE Photonics Technol. Lett. **32**(7), 391–394 (2020).
4. C. Belmonte, L. Frasunkiewicz, T. Czyszanowski, H. Thienpont, J. Beeckman, K. Neyts, and K. Panajotov, "Optimization of electrically tunable VCSEL with intracavity nematic liquid crystal," Opt. Express **23**(12), 15706–15715 (2015).
5. P. Debernardi, A. Simaz, A. Tibaldi, B. Boisnard, T. Camps, F. Bertazzi, M. Goano, B. Reig, J.-B. Doucet, and V. Bardinal, "Anisotropic transverse confinement design for electrically pumped 850 nm VCSELs tuned by an intra cavity liquid-crystal cell," IEEE J. Sel. Top. Quantum Electron. **28**(1), 1–11 (2022).
6. http://canaanchem.com/.
7. J. Li, S.-T. Wu, S. Brugioni, R. Meucci, and S. Faetti, "Infrared refractive indices of liquid crystals," J. Appl. Phys. **97**(7), 073501 (2005).
8. S.-T. Wu, C. Wu, M. Warenghem, and M. Ismaili, "Refractive index dispersions of liquid crystals," Opt. Eng. **32**(8), 1775–1780 (1993).
9. S. Brugioni, R. Meucci, and S. Faetti, "Refractive indices of liquid crystals E7 and K15 in the mid- and near-IR regions," J. Opt. Technol. (2006).
10. E. Garcia-Caurel, A. D. Martino, J.-P. Gaston, and L. Yan, "Application of spectroscopic ellipsometry and mueller ellipsometry to optical characterization," Appl. Spectrosc. **67**(1), 1–21 (2013).
11. A. Marino, V. Tkachenko, E. Santamato, N. Bennis, X. Quintana, J. Otón, and G. Abbate, "Measuring liquid crystal anchoring energy strength by spectroscopic ellipsometry," J. Appl. Phys. **107**(7), 073109 (2010).
12. N. Xie, H. Zhang, B. Liu, B. Song, and J. Wu, "Characterization of temperature-dependent refractive indices for nematic liquid crystal employing a microfiber-assisted mach–zehnder interferometer," J. Lightwave Technol. **35**(14), 2966–2972 (2017).
13. M. Kawaida, T. Yamaguchi, and T. Akahane, "Measurement of refractive indices of ferroelectric SmC*liquid crystal by the fabry-perot interference method," Jpn. J. Appl. Phys. **28**(Part 2, No. 9), L1602–L1605 (1989).
14. R. Ozaki, K. Nishi, T. Kan, and K. Kadowaki, "Simultaneous determination of ordinary and extraordinary refractive index dispersions of nematic liquid crystals in the visible and near-infrared regions from an interference spectrum," J. Appl. Phys. **120**(15), 155502 (2016).
15. E. Miszczyk, P. Morawiak, R. Mazur, M. Mrukiewicz, M. Olifierczuk, W. Piecek, Z. Raszewski, P. Kula, J. Kedzierski, J. Zielinski, and P. Harmata, "A direct assessment of refractive indices of nematic liquid crystals at broad VIS - MWIR range," Liq. Cryst. **45**(5), 703–714 (2018).
16. B. Sadani, B. Boisnard, X. Lafosse, T. Camps, J. Doucet, E. Daran, C. Paranthoen, C. Levallois, L. Dupont, S. Bouchoule, and V. Bardinal, "Liquid-crystal alignment by a nanoimprinted grating for wafer-scale fabrication of tunable devices," IEEE Photonics Technol. Lett. **30**(15), 1388–1391 (2018).
17. A. Simaz, B. Boisnard, T. Camps, J.-B. Doucet, B. Reig, A. Tibaldi, P. Debernardi, and V. Bardinal, "Thermal characterization of the birefringence of nematic liquid crystals for the design of widely-tunable LC-VCSELs," in *2020 International Conference on Numerical Simulation of Optoelectronic Devices (NUSOD)*, (2020), pp. 73–74.
18. T. Begou, F. Lemarchand, F. Lemarquis, A. Moreau, and J. Lumeau, "High-performance thin-film optical filters with stress compensation," J. Opt. Soc. Am. A **36**(11), C113–C121 (2019).
19. A. Tibaldi, P. Debernardi, and R. Orta, "Bimodal resonance phenomena. Part iii: high-contrast grating reflectors," IEEE J. Quantum Electron. **54**(6), 1–8 (2018).
20. Microchem, *Microchem SU-8 2000 Data Sheet* (2011).
21. Microchem, *Microchem Perminex 2000 Data Sheet* (2011).
22. C. Tan, "Determination of refractive index of silica glass for infrared wavelengths by IR spectroscopy," J. Non-Cryst. Solids **223**(1-2), 158–163 (1998).
23. L. Gao, F. Lemarchand, and M. Lequime, "Exploitation of multiple incidences spectrometric measurements for thin film reverse engineering," Opt. Express **20**(14), 15734–15751 (2012).
24. L. Gao, F. Lemarchand, and M. Lequime, "Refractive index determination of SiO_2 layer in the UV/vis/NIR range: spectrophotometric reverse engineering on single and bi-layer designs," J. Eur. Opt. Soc. - Rapid publ. **8**, 13010 (2013).
25. MATLAB (The MathWorks Inc., Natick, Massachusetts, 2020).
26. M. Magnello, "Chapter 56 - karl pearson, paper on the chi square goodness of fit test (1900)," in *Landmark Writings in Western Mathematics 1640-1940*, I. Grattan-Guinness, R. Cooke, L. Corry, P. Crépel, and N. Guicciardini, eds. (Elsevier Science, Amsterdam, 2005), pp. 724–731.